Journal of Systems Engineering and Electronics
Vol. 31, No. 6, December 2020, pp.1116 – 1127

Joint 2D-DOA and polarization estimation for sparse nonuniform rectangular array composed of spatially spread electromagnetic vector sensor

MA Huihui* and TAO Haihong

National Laboratory of Radar Signal Processing, Xidian University, Xi'an 710071, China

Abstract: In this paper, a sparse nonuniform rectangular array based on spatially spread electromagnetic vector sensor (SNRA-SSEMVS) is introduced, and a method for estimating 2D-direction of arrival (DOA) and polarization is devised. Firstly, according to the special structure of the sparse nonuniform rectangular array (SNRA), a set of accurate but ambiguous direction-cosine estimates can be obtained. Then the steering vector of spatially spread electromagnetic vector sensor (SSEMVS) can be extracted from the array manifold to obtain the coarse but unambiguous direction-cosine estimates. Finally, the disambiguation approach can be used to get the final accurate estimates of 2D-DOA and polarization. Compared with some existing methods, the SNRA configuration extends the spatial aperture and refines the parameters estimation accuracy without adding any redundant antennas, as well as reduces the mutual coupling effect. Moreover, the proposed algorithm resolves multiple sources without the priori knowledge of signal information, suffers no ambiguity in the estimation of the Poynting vector, and pairs the *x*-axis direction cosine with the *y*-axis direction cosine automatically. Simulation results are given to verify the effectiveness and superiority of the proposed algorithm.

Keywords: sparse nonuniform rectangular array (SNRA), spatially spread electromagnetic vector sensor (SSEMVS), direction-cosine, polarization, mutual coupling.

DOI: 10.23919/JSEE.2020.000084

1. Introduction

The electromagnetic vector sensor array is superior to the conventional scalar array [1,2] due to the polarization diversity, which can maximumly exploit the propagation information of the electromagnetic wave and improves the performance of the radar system. Direction of arrival (DOA) and polarization parameters estimation is a key issue of electromagnetic vector sensor array processing, which has drawn an increasing attention in the past decades. At the beginning, the DOA and polarization parameters estimation algorithm is only the extension of the DOA estimation method based on the conventional scalar array. For example, in [3−5], the traditional multiple signal classification (MUSIC) algorithm and the estimation of signal parameters via rotational invariance technique (ESPRIT) algorithm are extended to parameters estimation methods for the electromagnetic vector sensor array. Recently, some particular DOA and polarization parameters estimation techniques for electromagnetic vector sensor array have been developed. In [6−9], a vector-cross-product algorithm, which has low computational complexity, was proposed. In [10,11], the polarization smoothing algorithms were presented to cope with correlated sources. In [12−14], various parameters estimation algorithms based on quaternion algebra were developed, which are more robust to array error.

However, the array geometries in [6−14] were all based on the collocated electromagnetic vector sensor, which will introduce serious mutual coupling effect and sharply decrease the parameters estimation performance. To alleviate this problem, a spatially non-collocated electromagnetic vector sensor (SNC-EMVS) was proposed in [15], whose components are distributed along two parallel lines, which can reduce the mutual coupling effect. However, it is strict with the location of antenna components. To relax this condition, Li et al. [16] put forward a spatially spread electromagnetic vector sensor (SSEMVS) array, and a joint DOA and polarization parameters estimation algorithm was presented. However, it can only resolve five sources at most and has poor parameters estimation performance. To solve this problem, a sparse uniform array based on SNC-EMVS was proposed in [17], and a joint 2D-DOA and polarization parameters estimation method was devised, but it requires parameters pair matching operation, and has ambiguity in the estima-

Manuscript received October 21, 2019.
*Corresponding author.
This work was supported by the innovation project of Science and Technology Commission of the Central Military Commission.

tion of the Poynting vector, which causes unsatisfactory parameters estimation results. Considering the nonuniform sparse array, Wang et al. [18] presented a DOA estimation method for the nonuniform scalar L-shaped array, which requires pair-matching operation and has low parameters estimation accuracy. Moreover, it cannot measure the polarization information. On account of the shortcomings of the above methods, a sparse nonuniform rectangular array SSEMVS (SNRA-SSEMVS) is proposed in this paper, and an algorithm is devised accordingly. The proposed method avoids suffering ambiguity in the estimation of direction finding, pairs the parameters automatically, alleviates the mutual coupling effect and improves the estimation accuracy without adding any antennas. Moreover, the use of SSEMVS also relaxes the condition of array configuration in [17].

The rest of the paper is organized as follows. Section 2 introduces the signal model. In Section 3, the proposed method is described and a computational complexity comparison between the proposed method and the reduced dimensional (RD)-MUSIC is presented. In Section 4, simulations are conducted to validate the performance of our method. Section 5 draws the conclusion.

2. The proposed signal model

2.1 SSEMVS array geometry

The SSEMVS is composed of three orthogonal dipoles and three orthogonal loops that are spatially spread in space as shown in Fig. 1. The position vectors of the three orthogonal oriented dipole antennas and loop antennas are $\boldsymbol{P}_{ex}$, $\boldsymbol{P}_{ey}$, $\boldsymbol{P}_{ez}$, $\boldsymbol{P}_{hx}$, $\boldsymbol{P}_{hy}$ and $\boldsymbol{P}_{hz}$, respectively. The locations of all antennas need to satisfy the following relationship:

$$\begin{cases} \boldsymbol{P}_{ey}-\boldsymbol{P}_{ez}=-(\boldsymbol{P}_{hy}-\boldsymbol{P}_{hz}) \\ \boldsymbol{P}_{ez}-\boldsymbol{P}_{ex}=-(\boldsymbol{P}_{hz}-\boldsymbol{P}_{hx}) \\ \boldsymbol{P}_{ex}-\boldsymbol{P}_{ey}=-(\boldsymbol{P}_{hy}-\boldsymbol{P}_{hz}) \end{cases}. \tag{1}$$

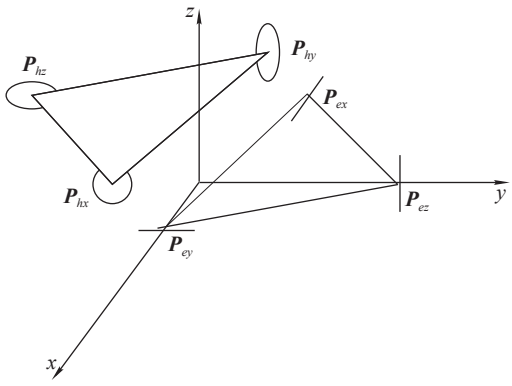

Fig. 1 Sketch of a single SSEMVS

The array steering vector $\tilde{\boldsymbol{a}}$ of SSEMVS can be written as

$$\tilde{\boldsymbol{a}}=\begin{bmatrix}\tilde{\boldsymbol{e}}\\ \tilde{\boldsymbol{h}}\end{bmatrix}=\underbrace{\begin{bmatrix} e^{j\frac{2\pi}{\lambda}\boldsymbol{P}_{ex}\cdot\boldsymbol{P}_s}\\ e^{j\frac{2\pi}{\lambda}\boldsymbol{P}_{ey}\cdot\boldsymbol{P}_s}\\ e^{j\frac{2\pi}{\lambda}\boldsymbol{P}_{ez}\cdot\boldsymbol{P}_s}\\ e^{j\frac{2\pi}{\lambda}\boldsymbol{P}_{hx}\cdot\boldsymbol{P}_s}\\ e^{j\frac{2\pi}{\lambda}\boldsymbol{P}_{hy}\cdot\boldsymbol{P}_s}\\ e^{j\frac{2\pi}{\lambda}\boldsymbol{P}_{hz}\cdot\boldsymbol{P}_s}\end{bmatrix}}_{\mathrm{d}(u,v)}\odot\boldsymbol{a}=$$

$$\underbrace{\begin{bmatrix} e^{j\frac{2\pi}{\lambda}(\boldsymbol{P}_{ex}(1)\sin\theta\cos\phi+\boldsymbol{P}_{ex}(2)\sin\theta\sin\phi+\boldsymbol{P}_{ex}(3)\cos\theta)}\\ e^{j\frac{2\pi}{\lambda}(\boldsymbol{P}_{ey}(1)\sin\theta\cos\phi+\boldsymbol{P}_{ey}(2)\sin\theta\sin\phi+\boldsymbol{P}_{ey}(3)\cos\theta)}\\ e^{j\frac{2\pi}{\lambda}(\boldsymbol{P}_{ez}(1)\sin\theta\cos\phi+\boldsymbol{P}_{ez}(2)\sin\theta\sin\phi+\boldsymbol{P}_{ez}(3)\cos\theta)}\\ e^{j\frac{2\pi}{\lambda}(\boldsymbol{P}_{hx}(1)\sin\theta\cos\phi+\boldsymbol{P}_{hx}(2)\sin\theta\sin\phi+\boldsymbol{P}_{hx}(3)\cos\theta)}\\ e^{j\frac{2\pi}{\lambda}(\boldsymbol{P}_{hy}(1)\sin\theta\cos\phi+\boldsymbol{P}_{hy}(2)\sin\theta\sin\phi+\boldsymbol{P}_{hy}(3)\cos\theta)}\\ e^{j\frac{2\pi}{\lambda}(\boldsymbol{P}_{hz}(1)\sin\theta\cos\phi+\boldsymbol{P}_{hz}(2)\sin\theta\sin\phi+\boldsymbol{P}_{hz}(3)\cos\theta)}\end{bmatrix}}_{\mathrm{d}(\theta,\phi)}\odot\boldsymbol{a}, \tag{2}$$

$$\boldsymbol{a}=\underbrace{\begin{bmatrix}\cos\phi\cos\theta & -\sin\phi\\ \sin\phi\cos\theta & \cos\phi\\ -\sin\theta & 0\\ -\sin\phi & -\cos\phi\cos\theta\\ \cos\phi & -\sin\phi\cos\theta\\ 0 & \sin\theta\end{bmatrix}}_{\overset{\mathrm{def}}{=}\boldsymbol{\Theta}(\theta,\phi)}\underbrace{\begin{bmatrix}\sin\gamma e^{j\eta}\\ \cos\gamma\end{bmatrix}}_{\overset{\mathrm{def}}{=}\boldsymbol{g}(\gamma,\eta)} \tag{3}$$

where $\tilde{\boldsymbol{e}}$ is the electric field vector, $\tilde{\boldsymbol{h}}$ is the magnetic field vector, $\boldsymbol{d}(u,v)$ is the spatial steering vector of SSEMVS, λ is the wavelength, and $\boldsymbol{P}_s=[u,v,w]^{\mathrm{T}}$ is the unit Poynting vector of the incident source with $u=\sin\theta\cos\phi$, $v=\sin\theta\sin\phi$ and $w=\cos\theta$ respresenting the impinging source's direction-cosines respectively along the x axis, the y axis, and the z axis. Herein, $\theta\in[0,\pi]$ denotes the incident source's elevation-angle, $\phi\in[0,2\pi)$ symbolizes the azimuth-angle, $\gamma\in\left[0,\frac{\pi}{2}\right]$ refers to the auxiliary polarization angle, $\eta\in[-\pi,\pi)$ represents the polarization phase difference, and $\odot$ symbolizes the element-wise multiplication between two vectors. Note that $\boldsymbol{\Theta}(\theta,\phi)$ depends only on the arrival-angles, whereas $\boldsymbol{g}(\gamma,\eta)$ depends only on the polarization parameters.

2.2 Structure of SNRA-SSEMVS

The SNRA composed of SSEMVS is depicted in Fig. 2, where the black dot represents the SSEMVS array. Consider K narrowband and independent signal sources impinging on this array, the received data of the (m,n)th SSEMVS at time t can be expressed as

$$\boldsymbol{x}_{m,n}(t)=\sum_{k=1}^{K}\tilde{\boldsymbol{a}}_k p_{m,n}(\theta_k,\phi_k)s_k(t)+\boldsymbol{n}_{m,n}(t) \tag{4}$$

where $\tilde{\boldsymbol{a}}_k$ is the steering vector of the kth signal of the (m,n)th SSEMVS; $p_{m,n}(\theta_k,\phi_k)=\mathrm{e}^{\mathrm{j}\frac{\pi}{\lambda}[m(m-1)D_X u_k+n(n-1)D_Y v_k]}$ is the phase shift factor, and the spacing between the first two adjacent SSEMVSs along the x axis and the y axis are D_X and D_Y, respectively; $s_k(t)$ is the kth signal; $\boldsymbol{n}_{m,n}(t)$ is a complex Gaussian white noise vector. The received signal can be expressed as

$$\begin{aligned}&\boldsymbol{x}(t)=\\&\left[\boldsymbol{x}_{1,1}^{\mathrm{T}}(t),\cdots,\boldsymbol{x}_{1,N}^{\mathrm{T}}(t),\cdots,\boldsymbol{x}_{M,1}^{\mathrm{T}}(t),\cdots;x_{M,N}^{\mathrm{T}}(t)\right]=\\&\sum_{k=1}^{K}\left[\boldsymbol{q}_x(u_k)\otimes\boldsymbol{q}_y(v_k)\otimes\widetilde{\boldsymbol{a}}_k\right]s_k(t)+\boldsymbol{n}(t)=\\&\sum_{k=1}^{K}\boldsymbol{b}_k s_k(t)+\boldsymbol{n}(t)=\boldsymbol{A}(u_k,v_k,\gamma_k,\eta_k)\boldsymbol{s}(t)+\boldsymbol{n}(t)\end{aligned}\tag{5}$$

where $\boldsymbol{b}_k$ represents the kth source's whole steering vector of the SNRA-SSEMVS, u_k and v_k denote the kth signal's direction cosines of x and y axes, γ_k and η_k denote the kth signal's auxiliary polarization angle and polarization phase difference. $\boldsymbol{q}_x(u_k)=[1,\mathrm{e}^{\mathrm{j}2\pi D_X\frac{u_k}{\lambda}},\cdots,\mathrm{e}^{\mathrm{j}\pi M(M-1)D_X\frac{u_k}{\lambda}}]^{\mathrm{T}}\in\mathbf{C}^{M\times 1}$ is the steering vector on the x axis, $\boldsymbol{q}_y(v_k)=[1,\mathrm{e}^{\mathrm{j}2\pi D_Y\frac{v_k}{\lambda}},\cdots,\mathrm{e}^{\mathrm{j}\pi N(N-1)D_Y\frac{v_k}{\lambda}}]^{\mathrm{T}}\in\mathbf{C}^{N\times 1}$ is the steering vector on the y axis, $\boldsymbol{s}(t)=[s_1(t),\cdots,s_K(t)]^{\mathrm{T}}\in\mathbf{C}^{K\times 1}$ is the signal vector, and $\boldsymbol{n}(t)\in\mathbf{C}^{6MN\times 1}$ is the additional Guassian white noise. The array manifold can be represented as

$$\begin{aligned}&\boldsymbol{A}(u_k,v_k,\gamma_k,\eta_k)=\\&[\boldsymbol{q}_x(u_1)\otimes\boldsymbol{q}_y(v_1)\otimes\tilde{\boldsymbol{a}}_1,\cdots,\boldsymbol{q}_x(u_K)\otimes\boldsymbol{q}_y(v_K)\otimes\tilde{a}_K]\in\mathbf{C}^{6MN\times K}\end{aligned}\tag{6}$$

where the superscript T represents the transpose operation and $\otimes$ symbolizes the kronecker product.

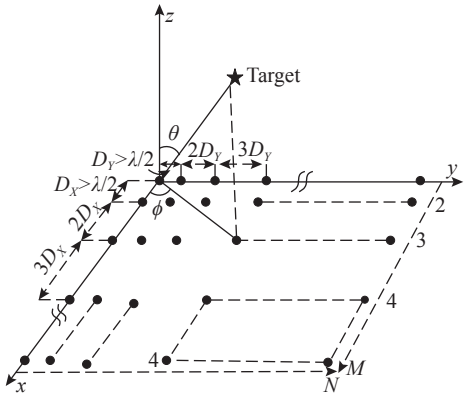

Fig. 2 Sketch of SNRA-SSEMVS

3. Algorithm description

Based on the array depicted in Section 2, a joint 2D-DOA and polarization estimation algorithm is proposed, and the procedure is shown in Fig. 3.

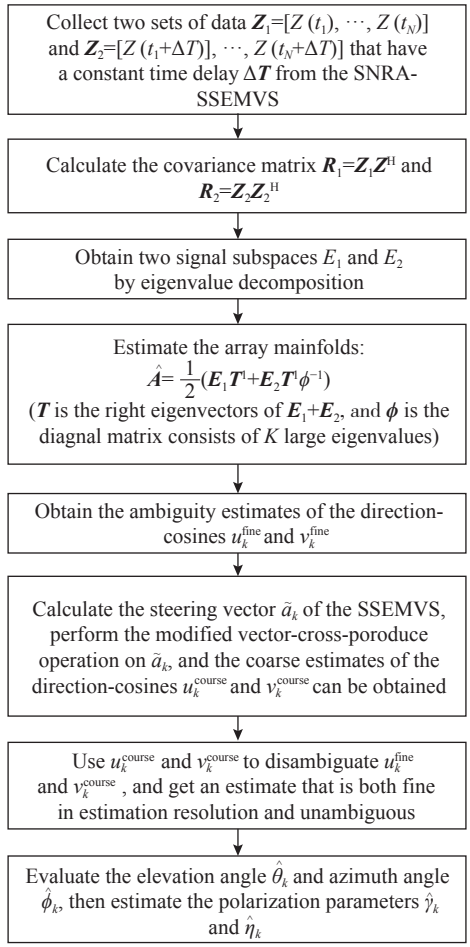

Fig. 3 Algorithm flowchart

In the proposed algorithm, the covariance matrix $\widehat{\boldsymbol{R}}$ can be calculated firstly, and the signal sub-spaces $\boldsymbol{E}_1$ and $\boldsymbol{E}_2$ can be obtained by the eigenvalue decomposition technique, then the array manifold $\widehat{\boldsymbol{A}}=\frac{1}{2}(\boldsymbol{E}_1\boldsymbol{T}^{-1}+\boldsymbol{E}_2\boldsymbol{T}^{-1}\boldsymbol{\phi}^{-1})$ can be estimated. Regard the whole nonuniform rectangular array as a set of line arrays parallel to the x axis, and all the line arrays on the plane can be converted to a line array located on the x axis by making phase compensation. According to the relationship among the elements on the x axis, the ambiguous direction-cosine estimate u_k^{fine} can be obtained. In a similar way, the ambiguous direction-cosine estimate v_k^{fine} can also be estimated. After extracting the steering vector $\widehat{\boldsymbol{a}}_k$ of the SSEMVS from $\widehat{\boldsymbol{A}}$, a pair of coarse direction-cosine estimates u_k^{course} and v_k^{course} can be derived by the modified vector cross-product algorithm. Next, the fine and unambiguous direction cosine estimates can be obtained by using the disambiguation approach. Finally, the high accurate estimation of 2D-DOA and polarization angles can be achieved.

3.1 Accurate but ambiguous direction cosine estimates based on ESPRIT

Uni-vector-sensor ESPRIT [16] forms a temporal invariance by two time-delayed sets of data collected from the SNRA-SSEMVS, the kth source impinging upon the array would contribute to two $6MN$ datasets. One is $\boldsymbol{b}_k s(t_n, f_k)$, $n = 1, \cdots, L$, and the other can be expressed as the following from:

$$\boldsymbol{b}_k s(t_n + \Delta T, f_k) = \boldsymbol{b}_k s(t_n, f_k) \mathrm{e}^{\mathrm{j}2\pi f_k \Delta T} \tag{7}$$

where the steering vector $\boldsymbol{b}_k$ is defined as in (5), ΔT is a constant time delay, and $s(t_n, f_k)$ has the following form:

$$s(t_n, f_k) = \sqrt{\boldsymbol{P}_k} \mathrm{e}^{\mathrm{j}(2\pi f_k t_n + \varphi_k)}, \quad k = 1, 2, \cdots, K \tag{8}$$

where $\boldsymbol{P}_k$, f_k, and φ_k are the power, frequency, and random phase of the kth source, respectively.

With a total of K incident sources and additive zero-mean white Gaussian noise, the received data of the nonuniform rectangular array can be written as

$$\boldsymbol{Z}(t_n) = \begin{bmatrix} \boldsymbol{A}_1 \\ \boldsymbol{A}_2 \end{bmatrix} \boldsymbol{s}(t_n) + \boldsymbol{n}(t_n) = \sum_{k=1}^{K} \begin{bmatrix} \boldsymbol{b}_k \boldsymbol{s}(t_n) \\ \boldsymbol{b}_k \mathrm{e}^{\mathrm{j}2\pi f_k \Delta T} \boldsymbol{s}(t_n) \end{bmatrix} + \boldsymbol{n}(t_n). \tag{9}$$

Then the entire $12MN \times L$ dataset can be expressed as

$$\boldsymbol{Z} = [\boldsymbol{Z}_{(t_1)}, \boldsymbol{Z}_{(t_2)}, \cdots, \boldsymbol{Z}_{(t_L)}] = \begin{bmatrix} \boldsymbol{Z}_1 \\ \boldsymbol{Z}_2 \end{bmatrix} \tag{10}$$

where $\boldsymbol{Z}_1$ and $\boldsymbol{Z}_2$ are the $6MN \times L$ datasets sampled at $\{t_1, \cdots, t_L\}$ and $\{t_1 + \Delta T, \cdots, t_L + \Delta T\}$, respectively. The two signal subspaces $\boldsymbol{E}_1$ and $\boldsymbol{E}_2$ can be estimated from $\boldsymbol{R}_1 = \boldsymbol{Z}_1 \boldsymbol{Z}_1^{\mathrm{H}}$ and $\boldsymbol{R}_2 = \boldsymbol{Z}_2 \boldsymbol{Z}_2^{\mathrm{H}}$ by selecting the eigenvectors associated with the largest K eigenvalues. A unique $K \times K$ nonsingular matrix $\boldsymbol{T}$ exists and relates $\boldsymbol{E}_i$ $(i = 1, 2)$ with the array manifold matrix as

$$\boldsymbol{E}_1 = \boldsymbol{A}_1 \boldsymbol{T}, \tag{11}$$

$$\boldsymbol{E}_2 = \boldsymbol{A}_2 \boldsymbol{T} = \boldsymbol{A}_1 \boldsymbol{\phi} \boldsymbol{T} \tag{12}$$

where $\boldsymbol{\phi} = \mathrm{diag}(\mathrm{e}^{\mathrm{j}2\pi f_1 \Delta T}, \cdots, \mathrm{e}^{\mathrm{j}2\pi f_K \Delta T})$. Based on (12), the following equation holds:

$$\boldsymbol{\psi} = \boldsymbol{E}_1^{+} \boldsymbol{E}_2 = \boldsymbol{T}^{-1} \boldsymbol{\phi} \boldsymbol{T} \tag{13}$$

where $+$ denotes the pseudo-inverse, $\boldsymbol{T}$ is the right eigenvector of $\boldsymbol{\psi}$, and the diagonal elements of $\boldsymbol{\phi}$ is composed of the eigenvalues of $\boldsymbol{\psi}$. Thus, the array manifold can be estimated as

$$\widehat{\boldsymbol{A}} = \frac{1}{2}(\boldsymbol{E}_1 \boldsymbol{T}^{-1} + \boldsymbol{E}_2 \boldsymbol{T}^{-1} \boldsymbol{\phi}^{-1}). \tag{14}$$

Moreover, the frequency estimation can be derived as

$$\widehat{f_k} = \frac{\mathrm{angle}([\boldsymbol{\phi}]_k)}{2\pi \Delta T}. \tag{15}$$

According to the estimation of array manifold, a matrix $\widehat{\boldsymbol{P}}_k$ that includes the spatial steering vector of the kth signal can be derived, with its (m, n)th element being

$$\widehat{\boldsymbol{P}}_k(m, n) = \mathrm{mean}\left\{\widehat{\boldsymbol{A}}\{[6(m-1)N + 6(n-1) + 1] : [6(m-1)N + 6n], k\} ./ \widehat{\boldsymbol{A}}(1:6, k)\right\}, \quad n = 1, 2, \cdots, N; m = 1, 2, \cdots, M; k = 1, 2, \cdots, K. \tag{16}$$

where $\boldsymbol{A}[m:n, k]$ represents a column vector composed of elements from the mth to the nth row of the kth column of the matrix $\boldsymbol{A}$. $\boldsymbol{A}./\boldsymbol{B}$ represents the division of corresponding elements of matrix $\boldsymbol{A}$ and matrix $\boldsymbol{B}$.

Then, vectorize the matrix $\widehat{\boldsymbol{P}}_k$ and make a transpose, and the spatial steering vector can be derived as

$$\widehat{\boldsymbol{b}}_k = (\mathrm{rvec}(\widehat{\boldsymbol{P}}_k))^{\mathrm{T}} = \begin{bmatrix} 1 \\ \mathrm{e}^{\mathrm{j}2\pi D_Y v_k / \lambda} \\ \vdots \\ \mathrm{e}^{\mathrm{j}\pi N(N-1) D_Y v_k / \lambda} \\ \mathrm{e}^{\mathrm{j}2\pi D_X u_k / \lambda} \\ \mathrm{e}^{\mathrm{j}2\pi (D_X u_k + D_Y v) / \lambda} \\ \vdots \\ \mathrm{e}^{\mathrm{j}(2\pi D_X u_k + \pi N(N-1) D_Y v_k) / \lambda} \\ \vdots \\ \mathrm{e}^{\mathrm{j}\pi M(M-1) D_X u_k / \lambda} \\ \vdots \\ \mathrm{e}^{\mathrm{j}\pi [M(M-1) D_X u_k + 2 D_Y v_k] / \lambda} \\ \mathrm{e}^{\mathrm{j}\pi [M(M-1) D_X u_k + N(N-1) D_Y v_k] / \lambda} \end{bmatrix}. \tag{17}$$

In order to get the estimation of the spatial steering vector $\boldsymbol{q}_{yk}$ along the y axis, the entire nonuniform rectangular array can be regarded as a combination of line arrays parallel to the the y axis, then by making phase compensation for each line array and making an average, $\boldsymbol{q}_{yk}$ can be obtained according to the following equations.

$$\boldsymbol{b}_{1k}(:, n) = \frac{\widehat{\boldsymbol{b}}_k[(n-1)N + 1 : nN]}{\widehat{\boldsymbol{b}}_k((n-1)N + 1)}, \quad n = 1, 2, \cdots, M \tag{18}$$

$$\boldsymbol{q}_{yk} = \frac{1}{M} \sum_{n=1}^{M} \boldsymbol{b}_{1k}(:, n) = \begin{bmatrix} 1 \\ \mathrm{e}^{\frac{\mathrm{j}2\pi D_Y v_k}{\lambda}} \\ \mathrm{e}^{\frac{\mathrm{j}2\pi (D_Y + 2D_Y) v_k}{\lambda}} \\ \vdots \\ \mathrm{e}^{\frac{\mathrm{j}\pi N(N-1) D_Y v_k}{\lambda}} \end{bmatrix} \tag{19}$$

Similarly, the entire array can also be considered as a combination of line arrays parallel to the x axis, then $\boldsymbol{q}_{xk}$ can be estimated as

$$\boldsymbol{b}_{2k}(:,m)=\frac{\widehat{\boldsymbol{b}}_k[m+(0:M-1)N]}{\widehat{\boldsymbol{b}}_k(m)},\quad m=1,2,\cdots,N, \tag{20}$$

$$\boldsymbol{q}_{xk}=\frac{1}{N}\sum_{m=1}^{N}\boldsymbol{b}_{2k}(:,m)=\begin{bmatrix}1\\ \mathrm{e}^{\frac{\mathrm{j}2\pi D_X u_k}{\lambda}}\\ \mathrm{e}^{\frac{\mathrm{j}2\pi(D_X+2D_X)u_k}{\lambda}}\\ \vdots\\ \mathrm{e}^{\frac{\mathrm{j}\pi M(M-1)D_X u_k}{\lambda}}\end{bmatrix}. \tag{21}$$

From (19) and (21), the accurate but ambiguous direction cosine estimates v_k^{fine} and u_k^{fine} can be obtained as follows:

$$\boldsymbol{b}_{yk1}=\boldsymbol{q}_{yk}(2:N)./\boldsymbol{q}_{yk}(1:N-1)=\begin{bmatrix}\mathrm{e}^{\mathrm{j}2\pi D_Y v_k/\lambda}\\ \mathrm{e}^{\mathrm{j}2\pi 2D_Y v_k/\lambda}\\ \vdots\\ \mathrm{e}^{\mathrm{j}2\pi(N-1)D_Y v_k/\lambda}\end{bmatrix}, \tag{22}$$

$$\boldsymbol{b}_{yk2}=\boldsymbol{b}_{xk1}(2:N-1)./\boldsymbol{b}_{xk1}(1:N-2)=\begin{bmatrix}\mathrm{e}^{\mathrm{j}2\pi D_Y v_k/\lambda}\\ \vdots\\ \mathrm{e}^{\mathrm{j}2\pi D_Y v_k/\lambda}\end{bmatrix}, \tag{23}$$

$$\boldsymbol{b}_{xk1}=\boldsymbol{q}_{xk}(2:M)./\boldsymbol{q}_{xk}(1:M-1)=\begin{bmatrix}\mathrm{e}^{\mathrm{j}2\pi D_X u_k/\lambda}\\ \mathrm{e}^{\mathrm{j}2\pi 2D_X u_k/\lambda}\\ \vdots\\ \mathrm{e}^{\mathrm{j}2\pi(M-1)D_X u_k/\lambda}\end{bmatrix}, \tag{24}$$

$$\boldsymbol{b}_{xk2}=\boldsymbol{b}_{xk1}(2:M-1)./\boldsymbol{b}_{xk1}(1:M-2)=\begin{bmatrix}\mathrm{e}^{\mathrm{j}2\pi D_X u_k/\lambda}\\ \vdots\\ \mathrm{e}^{\mathrm{j}2\pi D_X u_k/\lambda}\end{bmatrix}, \tag{25}$$

$$\boldsymbol{\psi}_{yk}=\text{mean}(\arg(\boldsymbol{b}_{yk2})), \tag{26}$$

$$\boldsymbol{\psi}_{y}=\text{diag}(\psi_{y1},\cdots,\psi_{yK}), \tag{27}$$

$$v_k^{\text{fine}}=\psi_{yk}\frac{\lambda}{2\pi D_Y},\quad k=1,2,\cdots,K, \tag{28}$$

$$\psi_{xk}=\text{mean}(\arg(\boldsymbol{b}_{xk2})), \tag{29}$$

$$\boldsymbol{\psi}_{x}=\text{diag}(\psi_{x1},\cdots,\psi_{xK}), \tag{30}$$

$$u_k^{\text{fine}}=\psi_{xk}\frac{\lambda}{2\pi D_X},\quad k=1,2,\cdots,K. \tag{31}$$

3.2 Coarse direction cosine estimates based on the modified vector-cross-product algorithm

It can be seen that the estimation of $\widehat{\boldsymbol{a}}_k$ can be derived from the first six rows of $\widehat{\boldsymbol{A}}$, and the estimation performance can be further improved by taking average of all the steering vector estimates of SSEMVS. Then the steering vector of SSEMVS $\widehat{\boldsymbol{a}}_k$ can be estimated as

$$\widehat{\boldsymbol{a}}_k=\frac{1}{MN}\sum_{m=1}^{M}\sum_{n=1}^{N}\widehat{\boldsymbol{A}}\{[6(m-1)N+6(n-1)+1]:[6(m-1)N+6n]\}[(\boldsymbol{\psi}_y)^*]^{\frac{n(n-1)}{2}}[(\boldsymbol{\psi}_x)^*]^{\frac{m(m-1)}{2}}\boldsymbol{e}_k \tag{32}$$

where $\boldsymbol{A}\{i:j\}$ is a matrix consisting of elements from the mth to the nth row of $\widehat{\boldsymbol{A}}$, the superscript $*$ denotes the complex conjugation, $\boldsymbol{e}_k=[\underbrace{0,\cdots,0}_{k-1},1,\underbrace{0,\cdots,0}_{K-k}]^{\mathrm{T}},k=1,\cdots,K$.

It was claimed in [16] that different directions of the incident signals can result in the same cross product vector when their unit Poynting vectors have the same modulus but different signs. To overcome this problem, Li et al. [16] proposed a modified vector-cross-product algorithm to avoid suffering ambiguity in the estimation of the unit Poynting vector. In the following, the brief procedure is provided.

Firstly, the normalized cross product $\boldsymbol{c}$ can be calculated from $\widehat{\boldsymbol{a}}_k$ with the vector-cross-product algorithm as follows:

$$\boldsymbol{c}=\frac{\tilde{\boldsymbol{e}}\cdot\tilde{\boldsymbol{h}}^*}{\|\tilde{\boldsymbol{e}}\|.\|\tilde{\boldsymbol{h}}^*\|}=\boldsymbol{P}_s\odot[\mathrm{e}^{\mathrm{j}\boldsymbol{g}_x\boldsymbol{P}_s}\quad\mathrm{e}^{\mathrm{j}\boldsymbol{g}_y\boldsymbol{P}_s}\quad\mathrm{e}^{\mathrm{j}\boldsymbol{g}_z\boldsymbol{P}_s}]^{\mathrm{T}} \tag{33}$$

where

$$\begin{cases}\boldsymbol{g}_x=-\dfrac{2\pi}{\lambda}(\boldsymbol{P}_{ey}-\boldsymbol{P}_{hz})\\ \boldsymbol{g}_y=-\dfrac{2\pi}{\lambda}(\boldsymbol{P}_{ez}-\boldsymbol{P}_{hx})\\ g_z=-\dfrac{2\pi}{\lambda}(\boldsymbol{P}_{ex}-\boldsymbol{P}_{hy})\end{cases}.$$

$\boldsymbol{P}_s$ is the unit Poynting vector of the incident source, $\boldsymbol{g}_x$, $\boldsymbol{g}_y$, and $\boldsymbol{g}_z$ are called $\boldsymbol{G}$ parameters of the SSEMVS. Owing to the ambiguous estimation of direction cosine in [15] and [17], the entry-wise modulus of $\boldsymbol{c}$ can be used to construct eight unit Poynting vectors, which can be expressed as

$$\boldsymbol{P}_{s1}=\begin{bmatrix}|[\boldsymbol{c}]_1|\\ |[\boldsymbol{c}]_2|\\ |[\boldsymbol{c}]_3|\end{bmatrix},\quad\boldsymbol{P}_{s2}=\begin{bmatrix}-|[\boldsymbol{c}]_1|\\ -|[\boldsymbol{c}]_2|\\ -|[\boldsymbol{c}]_3|\end{bmatrix},$$

$$\boldsymbol{P}_{s3}=\begin{bmatrix}|[\boldsymbol{c}]_1|\\ -|[\boldsymbol{c}]_2|\\ -|[\boldsymbol{c}]_3|\end{bmatrix},\quad\boldsymbol{P}_{s4}=\begin{bmatrix}-|[\boldsymbol{c}]_1|\\ |[\boldsymbol{c}]_2|\\ -|[\boldsymbol{c}]_3|\end{bmatrix},$$

$$\boldsymbol{P}_{s5}=\begin{bmatrix}-|[\boldsymbol{c}]_1|\\-|[\boldsymbol{c}]_2|\\|[\boldsymbol{c}]_3|\end{bmatrix},\quad \boldsymbol{P}_{s6}=\begin{bmatrix}|[\boldsymbol{c}]_1|\\|[\boldsymbol{c}]_2|\\-|[\boldsymbol{c}]_3|\end{bmatrix},$$

$$\boldsymbol{P}_{s7}=\begin{bmatrix}|[\boldsymbol{c}]_1|\\-|[\boldsymbol{c}]_2|\\|[\boldsymbol{c}]_3|\end{bmatrix},\quad \boldsymbol{P}_{s8}=\begin{bmatrix}-|[\boldsymbol{c}]_1|\\|[\boldsymbol{c}]_2|\\|[\boldsymbol{c}]_3|\end{bmatrix}. \tag{34}$$

Then substitute all of these vectors into (32) and choose the one with the least fitting error as the final estimation of the Poynting vector $\tilde{\boldsymbol{P}}_s$. Therefore, the coarse direction cosine estimates can be obtained as

$$\begin{cases}u_k^{\text{coarse}}=\left[\tilde{\boldsymbol{P}}_s\right]_1\\ v_k^{\text{coarse}}=\left[\tilde{\boldsymbol{P}}_s\right]_2\\ w_k^{\text{coarse}}=\left[\tilde{\boldsymbol{P}}_s\right]_3\end{cases}. \tag{35}$$

3.3 Yield of closed-form DOA and polarization estimates with high accuracy

By using the disambiguation approach [15], the final estimation of direction cosine can be achieved as

$$\begin{cases}\widehat{u}_k=u_k^{\text{fine}}+\widehat{m}\lambda/D_X\\ \widehat{m}=\arg_m\min|u_k^{\text{course}}-u_k^{\text{fine}}-m\lambda/D_X|\\ \lceil(-1-u_k^{\text{fine}})D_X/\lambda\rceil\leqslant m\leqslant\lfloor(1-u_k^{\text{fine}})D_X/\lambda\rfloor\\ \widehat{v}_k=v_k^{\text{fine}}+\widehat{n}\lambda/D_Y\\ \widehat{n}=\arg_n\min|v_k^{\text{course}}-v_k^{\text{fine}}-n\lambda/D_Y|\\ \lceil(-1-v_k^{\text{fine}})D_Y/\lambda\rceil\leqslant n\leqslant\lfloor(1-v_k^{\text{fine}})D_Y/\lambda\rfloor\end{cases} \tag{36}$$

where $\lceil\alpha\rceil$ refers to the smallest integer that is not less than α, and $\lfloor\alpha\rfloor$ refers to the largest integer that does not exceed α.

With the estimation of direction-cosine, the elevation and azimuth angles can be calculated subsequently. The following eight cases are discussed with the difference of Poynting vectors.

(i) If $\widehat{u}_k>0,\widehat{v}_k>0,\widehat{w}_k>0,\ k=1,2,\cdots,K$

$$\widehat{\theta}_k=\arcsin\left(\sqrt{\widehat{u}_k^2+\widehat{v}_k^2}\right)$$
$$\widehat{\phi}_k=\arctan\left(\frac{\widehat{v}_k}{\widehat{u}_k}\right) \tag{37}$$

(ii) If $\widehat{u}_k<0,\widehat{v}_k<0,\widehat{w}_k<0,\ k=1,2,\cdots,K$

$$\widehat{\theta}_k=\pi-\arcsin\left(\sqrt{\widehat{u}_k^2+\widehat{v}_k^2}\right)$$
$$\widehat{\phi}_k=\arctan\left(\frac{\widehat{v}_k}{\widehat{u}_k}\right) \tag{38}$$

(iii) If $\widehat{u}_k<0,\widehat{v}_k<0,\widehat{w}_k>0,\ k=1,2,\cdots,K$

$$\widehat{\theta}_k=\arcsin\left(\sqrt{\widehat{u}_k^2+\widehat{v}_k^2}\right)$$
$$\widehat{\phi}_k=\pi+\arctan\left(\frac{\widehat{v}_k}{\widehat{u}_k}\right) \tag{39}$$

(iv) If $\widehat{u}_k<0,\widehat{v}_k>0,\widehat{w}_k>0,\ k=1,2,\cdots,K$

$$\widehat{\theta}_k=\pi-\arcsin\left(\sqrt{\widehat{u}_k^2+\widehat{v}_k^2}\right)$$
$$\widehat{\phi}_k=\pi+\arctan\left(\frac{\widehat{v}_k}{\widehat{u}_k}\right) \tag{40}$$

(v) If $\widehat{u}_k>0,\widehat{v}_k<0,\widehat{w}_k<0,\ k=1,2,\cdots,K$

$$\widehat{\theta}_k=\pi-\arcsin\left(\sqrt{\widehat{u}_k^2+\widehat{v}_k^2}\right)$$
$$\widehat{\phi}_k=\arctan\left(\frac{\widehat{v}_k}{\widehat{u}_k}\right) \tag{41}$$

(vi) If $\widehat{u}_k<0,\widehat{v}_k>0,\widehat{w}_k>0,\ k=1,2,\cdots,K$

$$\widehat{\theta}_k=\arcsin\left(\sqrt{\widehat{u}_k^2+\widehat{v}_k^2}\right)$$
$$\widehat{\phi}_k=\pi+\arctan\left(\frac{\widehat{v}_k}{\widehat{u}_k}\right) \tag{42}$$

(vii) If $\widehat{u}_k>0,\widehat{v}_k<0,\widehat{w}_k>0,\ k=1,2,\cdots,K$

$$\widehat{\theta}_k=\arcsin\left(\sqrt{\widehat{u}_k^2+\widehat{v}_k^2}\right)$$
$$\widehat{\phi}_k=\arctan\left(\frac{\widehat{v}_k}{\widehat{u}_k}\right) \tag{43}$$

(viii) If $\widehat{u}_k>0,\widehat{v}_k>0,\widehat{w}_k<0,\ k=1,2,\cdots,K$

$$\widehat{\theta}_k=\pi-\arcsin\left(\sqrt{\widehat{u}_k^2+\widehat{v}_k^2}\right)$$
$$\widehat{\phi}_k=\arctan\left(\frac{\widehat{v}_k}{\widehat{u}_k}\right) \tag{44}$$

Also from (3),

$$\widehat{\boldsymbol{g}}(\gamma_k,\eta_k)=\left[\boldsymbol{\Theta}^{\mathrm{H}}\left(\widehat{\theta}_k,\widehat{\phi}_k\right)\boldsymbol{\Theta}\left(\widehat{\theta}_k,\widehat{\phi}_k\right)\right]^{-1}\cdot\boldsymbol{\Theta}^{\mathrm{H}}\left(\widehat{\theta}_k,\widehat{\phi}_k\right)\left[\widehat{\boldsymbol{a}}_k\odot\boldsymbol{d}^*\left(\widehat{u}_k,\widehat{v}_k\right)\right]. \tag{45}$$

As a result, the corresponding polarization parameters can be estimated as

$$\widehat{\gamma}_k=\arctan\left(\frac{[\widehat{\boldsymbol{g}}(\gamma_k,\eta_k)]_1}{[\widehat{\boldsymbol{g}}(\gamma_k,\eta_k)]_2}\right), \tag{46}$$

$$\widehat{\eta}_k=\angle\left[\frac{[\widehat{\boldsymbol{g}}(\gamma_k,\eta_k)]_1}{[\widehat{\boldsymbol{g}}(\gamma_k,\eta_k)]_2}\right] \tag{47}$$

where $\angle$ denotes the angle of the ensuring entity.

3.4 Computational complexity analysis

The main computational complexity of the proposed method includes: (i) calculation of array covariance mat-

rix with $O\{(12MN)^2L\}$ flops, (ii) eigen decomposition operation to obtain signal subspaces with $O\{(12MN)^3\}$ flops, (iii) estimation of the array manifolds with $O\{[2\cdot 6MNK^2+K^3]+4\cdot 6MNK^2+K^3\}$ flops, (iv) estimation of the array manifold for SSEMVS array with $O\{3MN\cdot 6K^2\}$ flops. Overall, the computational load of the proposed algorithm is $O\{(12MN)^2L+(12MN)^3+2K^3+54MNK^2\}$.

Table 1 shows the computational complexity comparison of the reduced dimensional polarimetric MUSIC algorithm (RD-MUSIC) and the proposed algorithm, where $\Delta\theta$ is the search range of elevation angle, and $\Delta\phi$ is the search range of azimuth angle. It can be seen that the computational complexity of the proposed algorithm is relatively lower.

Table 1 Computational complexity of the proposed algorithm and RD-MUSIC

Algorithm	Computational complexity
The proposed algorithm	$O\{(12MN)^2L+(12MN)^3+2K^3+54MNK^2\}$
RD-MUSIC	$O\{[(180/\Delta\theta)\cdot(360/\Delta\phi)\cdot(MN+MN\cdot 12+6MN(12MN-K)+2(12MN-K)\cdot 6MN+24MN+2^3)]+3MN\cdot 6K^2+(12MN)^2L+(12MN)^3+[2\cdot 6MNK^2+K^3]+4\cdot 6MNK^2+K^3\}$

4. Simulation results

In this section, several simulations are conducted to validate the performance of the proposed algorithm. In the following simulations, the configuration of SSEMVS is shown in Fig. 4. Stars refer to dipole antennas, circles denote the loop antennas. The corresponding parameters $\boldsymbol{G}=[\boldsymbol{g}_x\ \ \boldsymbol{g}_y\ \ \boldsymbol{g}_z]^{\mathrm{T}}$ is of the following form:

$$\boldsymbol{G}=\begin{bmatrix}0&1&0\\0&0&1\\1&0&0\end{bmatrix}\frac{2\pi}{\lambda}.$$

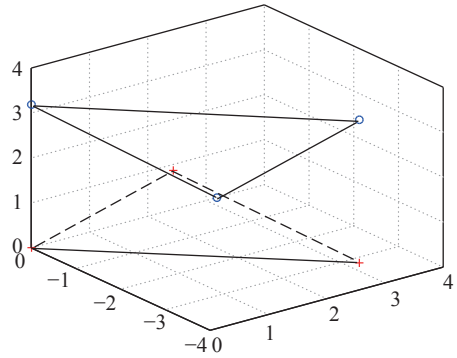

Fig. 4 Geometry illustrations of SSEMVS

4.1 Four-dimensional parameters estimation and pairing

It is assumed that the size of the SNRA is 5×6, $M=5$ and $N=6$. The SNR is set as 20 dB, and the number of snapshots is $L=500$. We consider $K=7$ targets,

$$(\theta_1,\phi_1,\gamma_1,\eta_1,f_1)=(10^\circ,35^\circ,70^\circ,30^\circ,0.1\ \text{Hz}),$$

$$(\theta_2,\phi_2,\gamma_2,\eta_2,f_2)=(20^\circ,65^\circ,60^\circ,120^\circ,0.2\ \text{Hz}),$$

$$(\theta_3,\phi_3,\gamma_3,\eta_3,f_3)=(80^\circ,55^\circ,50^\circ,60^\circ,0.3\ \text{Hz}),$$

$$(\theta_4,\phi_4,\gamma_4,\eta_4,f_4)=(40^\circ,15^\circ,40^\circ,110^\circ,0.4\ \text{Hz}),$$

$$(\theta_5,\phi_5,\gamma_5,\eta_5,f_5)=(50^\circ,85^\circ,30^\circ,80^\circ,0.5\ \text{Hz}),$$

$$(\theta_6,\phi_6,\gamma_6,\eta_6,f_6)=(60^\circ,45^\circ,20^\circ,140^\circ,0.6\ \text{Hz}),$$

$$(\theta_7,\phi_7,\gamma_7,\eta_7,f_7)=(70^\circ,25^\circ,10^\circ,40^\circ,0.7\ \text{Hz}).$$

A total of 100 Monte Carlo simulations are conducted and the results are shown in Fig. 5. It can be seen that the DOA and polarization angles are well estimated and correctly paired.

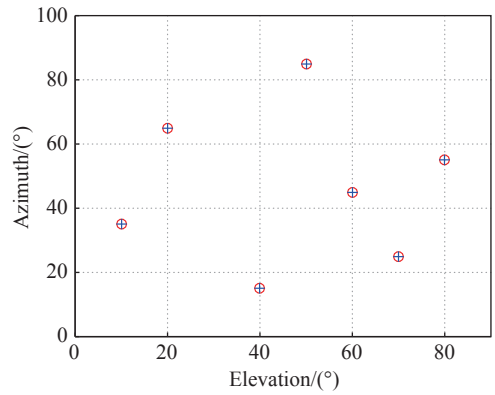

(a) Azimuth and elevation angles estimations and pairing

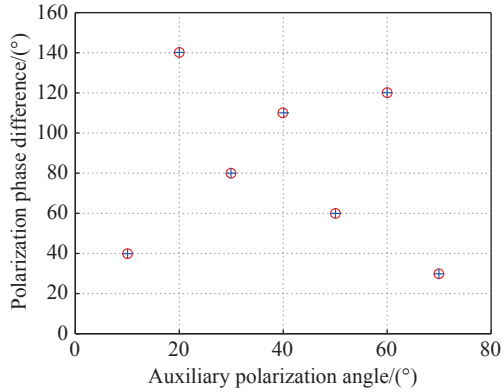

(b) Auxiliary polarization angle and polarization phase difference angle estimations and pairing

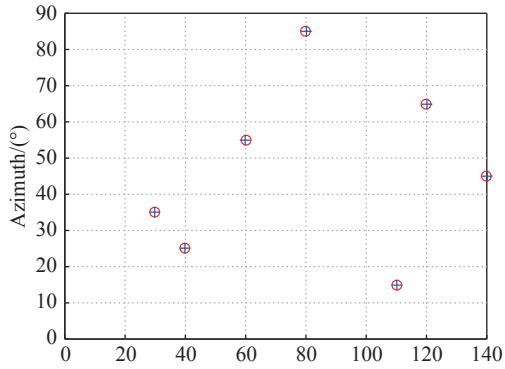

(c) Azimuth angle and polarization phase difference angle estimations and pairing

○ : Estimated value; + : True value.

Fig. 5 Four-dimensional parameters estimations of the proposed algorithm

4.2 Parameters estimation performance versus SNR

Suppose $M=5$, $N=6$, $D_X=4\lambda$, $D_Y=8\lambda$, and suppose there are two sources with

$$(\theta_1,\phi_1,\gamma_1,\eta_1,f_1)=(-35^\circ,42^\circ,45^\circ,-90^\circ,0.1\text{ Hz})$$

and

$$(\theta_2,\phi_2,\gamma_2,\eta_2,f_2)=(43^\circ,-35^\circ,45^\circ,90^\circ,0.126\,5\text{ Hz}),$$

$L=500$, $\Delta T=\dfrac{1}{2f_2}$, and the simulation results are obtained by 1 000 Monte Carlo experiments. The root mean squared error (RMSE) can be used to measure the estimation performance, which is defined as

$$\text{RMSE}=\sqrt{\frac{1}{1\,000K}\sum_{k=1}^{K}\sum_{j=1}^{1\,000}(\alpha_k-\tilde{\alpha}_{k,j})^2} \tag{48}$$

where $\tilde{\alpha}_{k,j}$ is the estimated α_k in which k denotes the target number and j denotes the trail number. Fig. 6 compares the RMSEs versus signal to noise ratio (SNR) of the proposed algorithm with the RD-MUSIC.

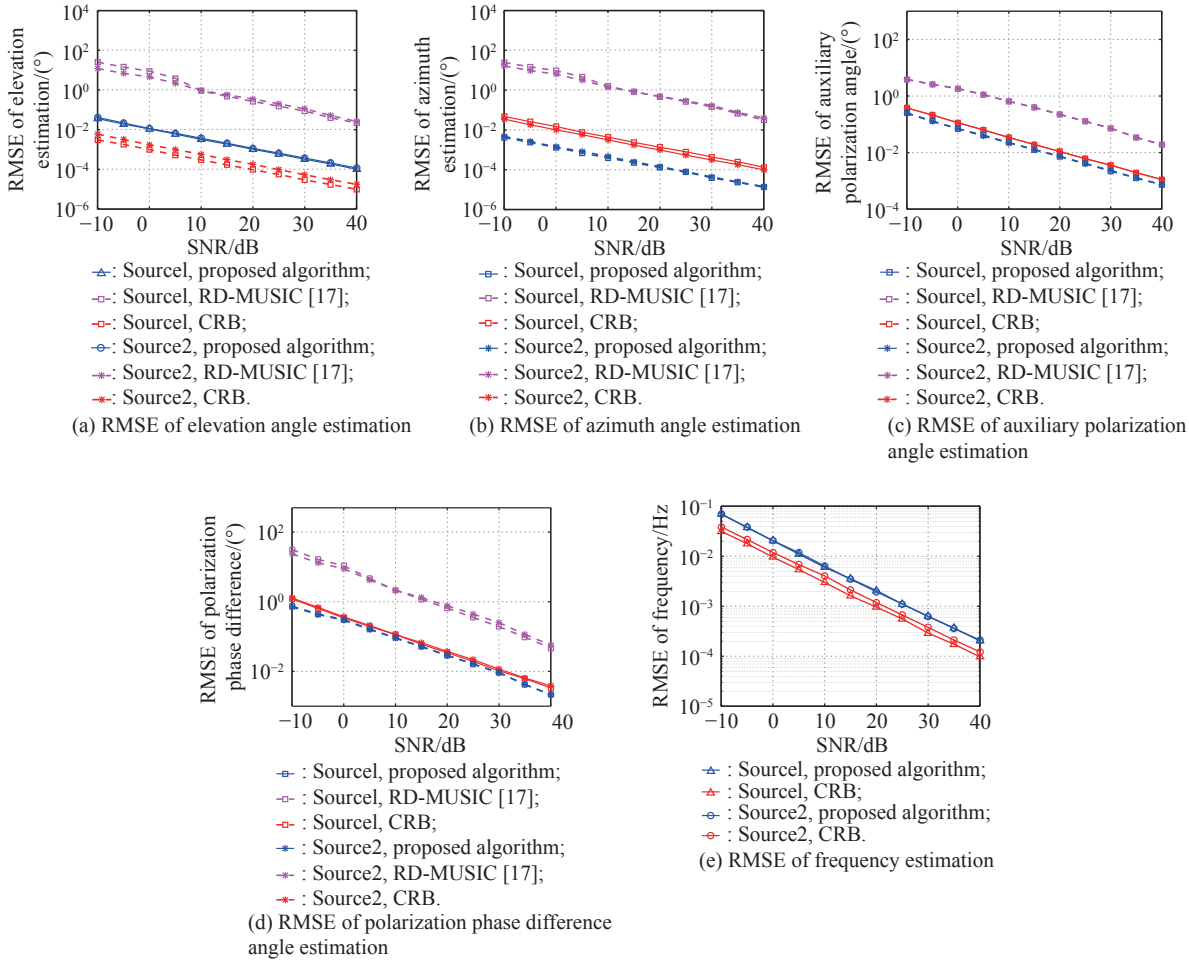

(a) RMSE of elevation angle estimation

(b) RMSE of azimuth angle estimation

(c) RMSE of auxiliary polarization angle estimation

(d) RMSE of polarization phase difference angle estimation

(e) RMSE of frequency estimation

Fig. 6 RMSEs versus SNR of parameters estimation

It can be seen that the parameters estimation performance of the proposed algorithm is superior to the RD-MUSIC in [17] and can approach to the Cramér-Rao bounds (CRBs) more effectively. It is worth mentioning that the parameters estimation performance of the RD-MUSIC is unsatisfactory when the SNR is lower than 5dB. However, for our proposed method, it can provide a high parameters estimation accuracy even at low SNRs.

4.3 Parameters estimation performance versus the number of data samples

The SNR is fixed at 20 dB, and the other settings are the same as those in Section 4.2. When the number of snapshots varies from 200 to 1 200, the RMSEs of parameter estimations are shown in Fig. 7. Again, it is seen that the proposed algorithm still has obvious advantages over the RD-MUSIC for all available snapshots and approaches to the related CRBs more effectively.

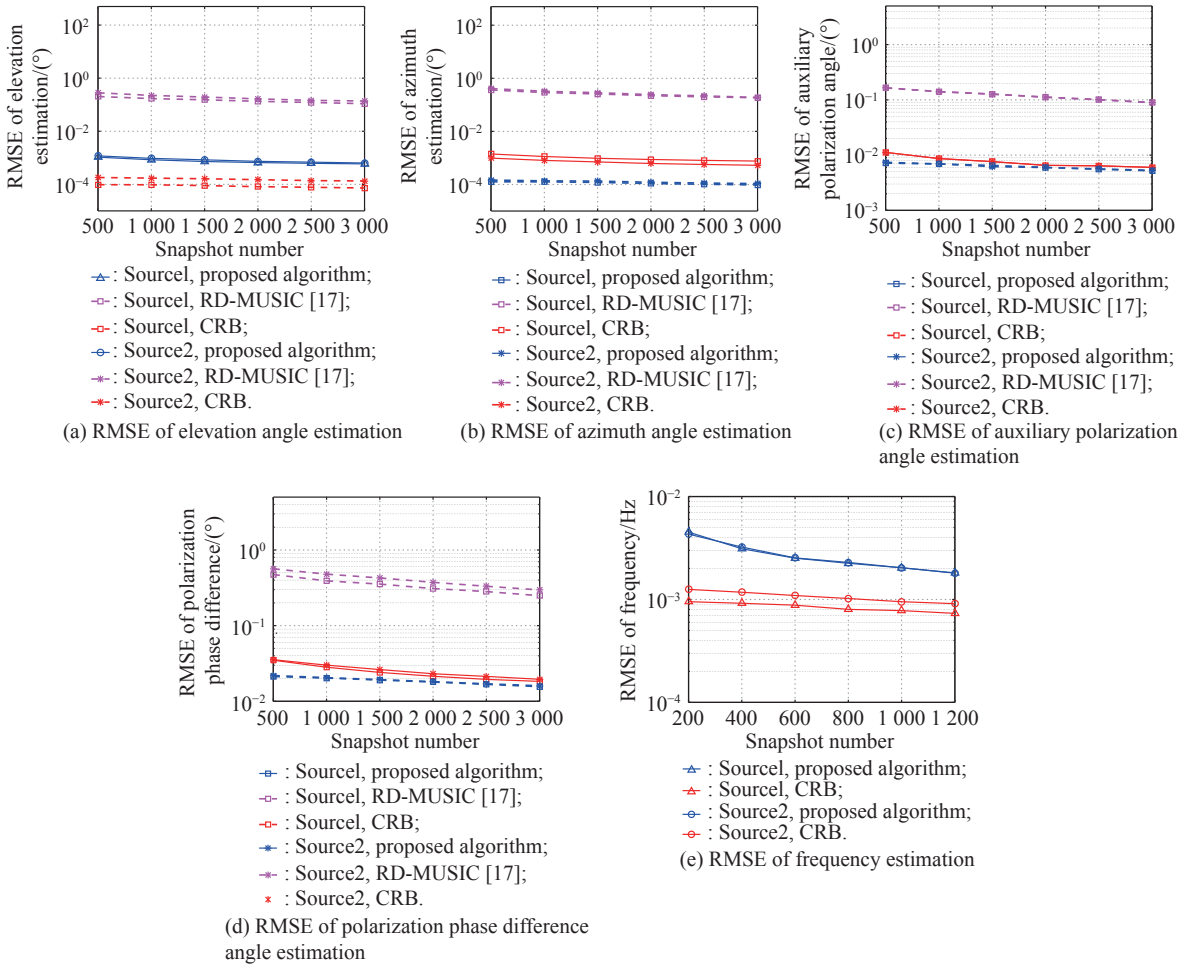

(a) RMSE of elevation angle estimation

(b) RMSE of azimuth angle estimation

(c) RMSE of auxiliary polarization angle estimation

(d) RMSE of polarization phase difference angle estimation

(e) RMSE of frequency estimation

Fig. 7 RMSEs versus snapshots of parameters estimation

4.4 Parameters estimation performance of different array structures

In this section, the CRBs of the proposed array is compared with three different array configurations presented in [16−18], respectively. Fig. 8 plots the RMSEs versus $D_X = D_Y$, the SNR is fixed as 20 dB, and other simulation conditions are the same as those in Section 4.2. Fig. 9 describes the RMSEs versus SNR, and other settings are fixed as those in Section 4.2. As it can be seen, the 2D-DOA estimation performance gets better when the inter-sensor spacing gets larger, while the RMSEs of the polarization parameters estimation remain the same with the increase of intersensor spacing. From Fig. 8 and Fig. 9, we can also see that the proposed algorithm has obvious advantages over the other methods. The reason is that the sparse nonuniform array configuration extends the array aperture and hence refines the parameter estimation accuracy.

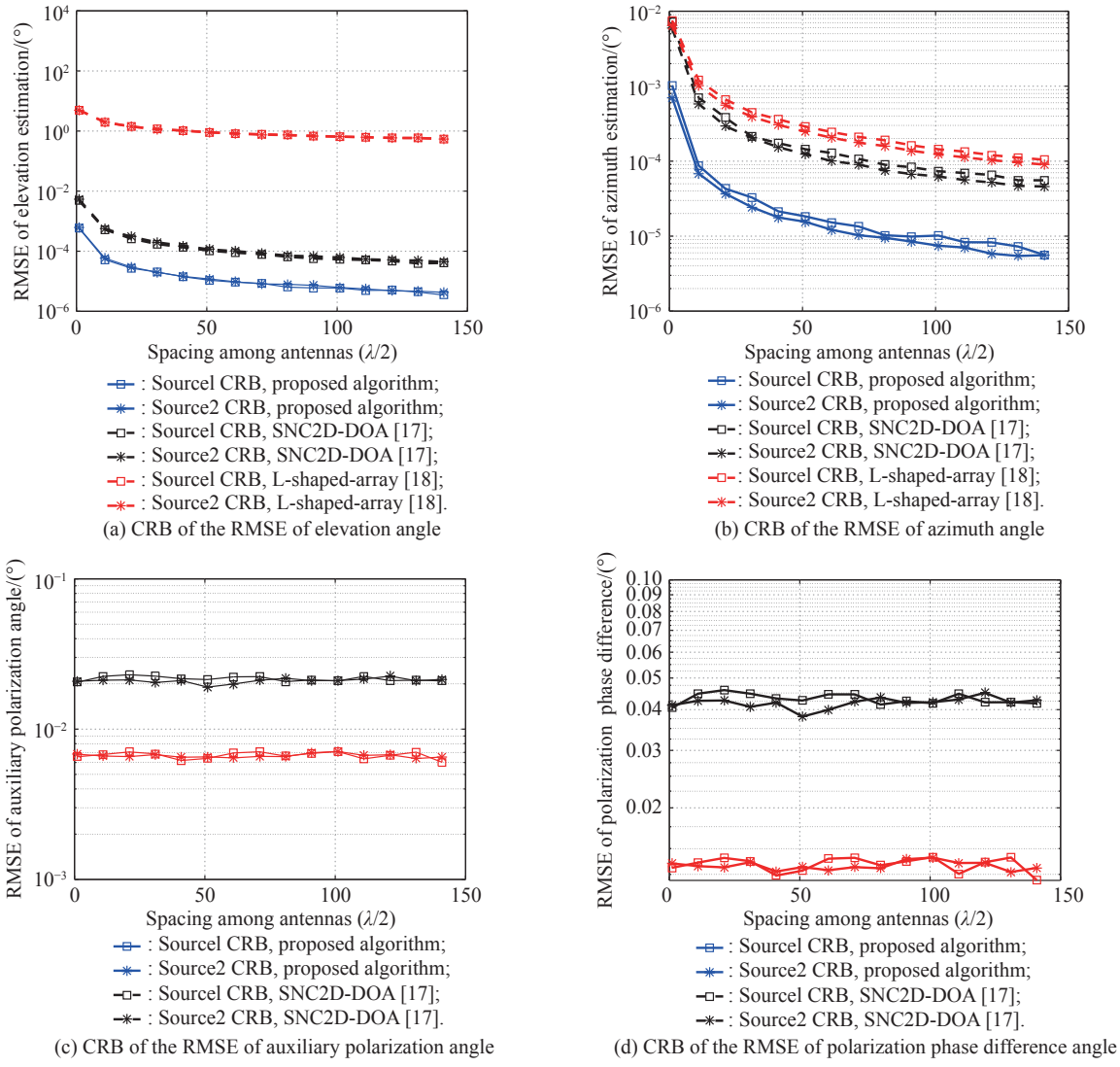

(a) CRB of the RMSE of elevation angle

(b) CRB of the RMSE of azimuth angle

(c) CRB of the RMSE of auxiliary polarization angle

(d) CRB of the RMSE of polarization phase difference angle

Fig. 8 CRBs of the four-dimensional parameters estimation versus intersensor spacing of L-shaped array, SNC-EMVS, and the proposed array

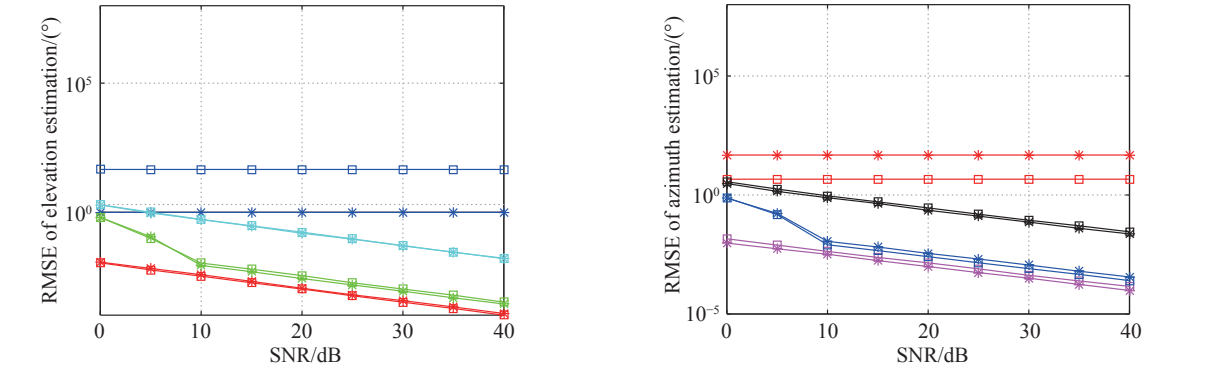

(a) CRB versus SNR of elevation angle estimation

(b) CRB versus SNR of azimuth angle estimation

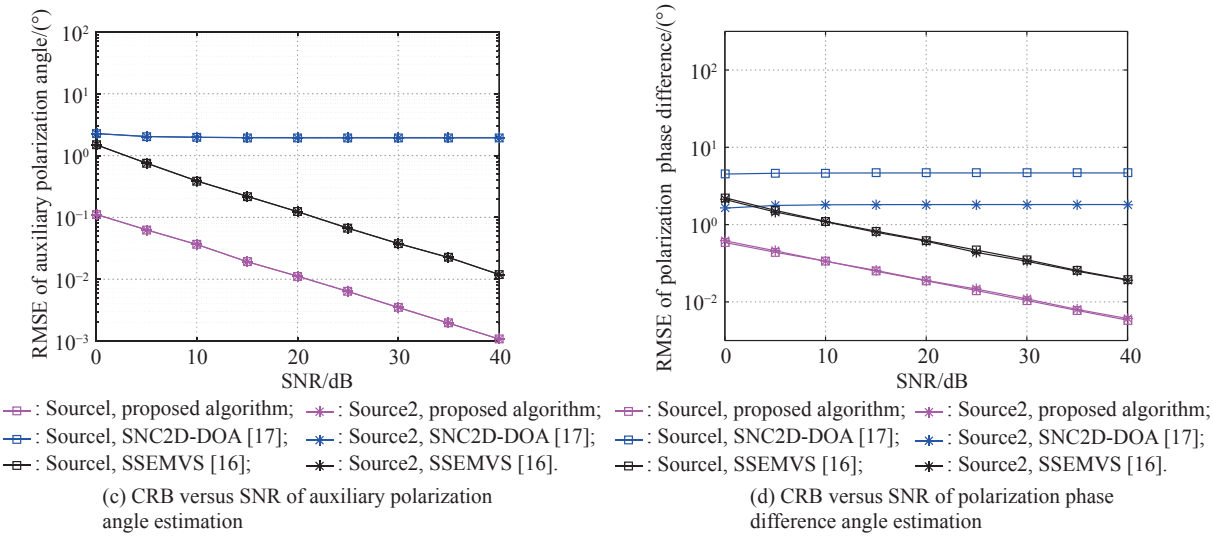

(c) CRB versus SNR of auxiliary polarization angle estimation

(d) CRB versus SNR of polarization phase difference angle estimation

Fig. 9 CRBs of four-dimensional parameters estimations versus SNR of SSEMVS, L-shape array, SNC-EMVS, and the proposed array

Moreover, compared to the method in [17], the mutual coupling effect and hardware cost can also be reduced. The reason for the unsatistactory parameters estimation performance in [17] is that there exists ambiguity in the estimation of the unit Poynting vector, which leads to the incorrect estimation of 2D-DOA and polarization angles.

5. Conclusions

In this paper, a method has been developed for 2D-DOA and polarization estimation in the SNRA composed of SSEMVS. Compared with some existing methods, the proposed one avoids suffering ambiguity in the estimation of direction finding, improves the parameters estimation accuracy without adding any redundant antennas, and reduces the mutual coupling effect. Moreover, compared to RD-MUSIC, the proposed method has relatively lower computational complexity. In addition, the 2D-DOA and polarization angles can also be paired automatically.

References

[1] ZHAO J, TAO H. Quaternion based joint DOA and polarization parameters estimation with stretched three-component electromagnetic vector sensor array. Journal of Systems Engineering and Electronics, 2017, 28(1): 5–13.

[2] DIAO M, AN C. Direction finding of coexisted independent and coherent signals using electromagnetic vector sensor. Journal of Systems Engineering and Electronics, 2012, 23(4): 481–487.

[3] CHENG Q, HUA Y B. Performance analysis of the MUSIC and Pencil-MUSIC algorithms for diversity polarized array. IEEE Trans. on Signal Processing, 1994, 42(11): 3150–3165.

[4] LI J, COMPTON R T. Angle and polarization estimation using ESPRIT with a polarization sensitive array. IEEE Trans. on Antennas and Propagation, 1991, 39(9): 1376–1383.

[5] ROY R, KAILATH T. ESPRIT-estimation of signal parameters via rotational invariance techniques. IEEE Trans. on Acoustics, Speech and Signal Processing, 1989, 37(7): 984–995.

[6] NEHORAI A, PALDI E. Vector sensor array processing for electromagnetic source localization. IEEE Trans. on Signal Processing, 1994, 42(2): 376–398.

[7] WONG K T, YUAN X. Vector cross-product direction-finding with an electromagnetic vector-sensor of six orthogonally oriented but spatially noncollocating dipoles. IEEE Trans. on Signal Processing, 2011, 59(1): 160–171.

[8] KAINAM T, ZOLTOWSKI M D. Uni-vector-sensor ESPRIT for multisource azimuth, elevation, and polarization estimation. IEEE Trans. on Antennas and Propagation, 1997, 45(10): 1467–1474.

[9] HO K C, TAN K C, SER W. An investigation on number of signals whose directions of arrival are uniquely determinable with an electromagnetic vector sensor. Signal Processing, 1995, 47(1): 41–54.

[10] RAHAMIM D, TABRIKIAN J, SHAVIT R. Source localization using vector sensor array in a multipath environment. IEEE Trans. on Signal Processing, 2004, 52(11): 3096–3103.

[11] XU Y G, LIU Z W. Polarimetric angular smoothing algorithm for an electromagnetic vector-sensor array. IET Radar, Sonar, & Navigation, 2008, 1(3): 230–240.

[12] WANG G B, TAO H H, WANG L M, et al. Joint estimation of DOA and polarization with COLD pair cylindrical array based on quaternion model. Mathematical Problems in Engineering, 2014. DOI: 10.1155/2014/806853.

[13] BIHAN N L, MIRON S, MARS J I. MUSIC algorithm for vector-sensors array using biquaternions. IEEE Trans. on Signal Processing, 2007, 55(9): 4523–4533.

[14] SCHULR D, THOMA R S. Quaternion-based polarimetric

array manifold interpolation. Signal Processing, 2015, 108(3): 245–258.

[15] WONG K T, YUAN X. Vector cross-product direction-finding with an electromagnetic vector-sensor of six orthogonally oriented but spatially noncollocating dipoles/loops. IEEE Trans. on Signal Processing, 2014, 62(4): 1028–1030.

[16] LI Y, ZHANG J Q. An enumerative nonlinear programming approach to direction finding with a general spatially spread electromagnetic vector sensor array. Signal Processing, 2013, 93(4): 856–865.

[17] ZHENG G M, CHEN B X, YANG M L, et al. Joint 2D-DOA and polarization estimation using a sparse uniform array of spatially non-collocating electromagnetic vector sensors. Scientia Sinica, 2014, 44(9): 1171–1192. (in Chinese)

[18] WANG L M, CHEN Z H, WANG G B. High resolution DOA estimation algorithm based on nonuniform L-shaped array. Proc. of the 2nd International Conference on Advances in Computer Science and Engineering, 2013, 53(3): 54–58.

Biographies

MA Huihui was born in 1993. She received her B.E. degree in electronic information engineering from Zhengzhou University in 2015. She is currently pursuing her doctor's degree with the National Laboratory of Radar Signal Processing, Xidian University. Her research interests include MIMO radar and vector sensor array signal processing.
E-mail: 1981734461@qq.com

TAO Haihong was born in 1976. She received her M.S. and Ph.D. degrees from the School of Electronic Engineering, Xidian University, Xi'an, China, in 2000 and 2004, respectively. She is currently a professor of the School of Electronic Engineering, Xidian University. She is also serving as the director of the National Laboratory of Radar Signal Processing at Xidian University. Her research interests include radar signal processing and detection, high-speed real-time signal processing, and array signal processing.
E-mail: hhtao@xidian.edu.cn